Atom-specific magnon-driven ultrafast spin dynamics in $Fe_{1-x}Ni_x$ alloys

Somnath Jana [●],[1,*] Ronny Knut [●],[1,†] Erna K. Delczeg-Czirjak,[1] Rameez S. Malik,[1] Robert Stefanuik,[1]
Joachim A. Terschlüsen,[1] Raghuveer Chimata,[1] Dibya Phuyal,[1] M. Venkata Kamalakar,[1] Serkan Akansel,[2]
Daniel Primetzhofer,[1] Martina Ahlberg,[3] Johan Söderström,[1] Johan Åkerman,[3,4] Peter Svedlindh,[2] Olle Eriksson,[1]
and Olof Karis[1]

[1]*Department of Physics and Astronomy, Uppsala University, Box 516, 75120 Uppsala, Sweden*
[2]*Department of Engineering Sciences, Uppsala University, Box 534, 75121 Uppsala, Sweden*
[3]*Department of Physics, University of Gothenburg, 412 96 Gothenburg, Sweden*
[4]*Department of Applied Physics, School of Engineering Sciences, KTH Royal Institute of Technology,
164 40 Kista, Sweden*

By employing element-specific spectroscopy in the ultrafast time scale in $Fe_{1-x}Ni_x$ alloys, we find a composition-dependent effect in the demagnetization that we relate to electron-magnon scattering and changes in the spin-wave stiffness. In all six measured alloys of different composition, the demagnetization of Ni compared to Fe exhibits a delay, an effect which we find is inherent in alloys but not in elemental Fe and Ni. Using a model based on electron-magnon scattering, we extract a spin-wave stiffness from all alloys that show excellent agreement with values obtained from other techniques.

Since the first observation of ultrafast magnetization quenching in Ni [1], a central topic has been to understand the possible channels of angular momentum dissipation from the spin system. Several theoretical models have been employed along with numerous experimental techniques [2–6]. Elliott-Yafet (EY) spin-flip processes through electron-phonon scattering can transfer the angular momentum from the spin to the lattice via the spin-orbit interaction, which is often used to describe ultrafast demagnetization [7–11]. Several recent studies, by means of femtosecond x-ray photoemission and x-ray and electron diffraction [12–14], have investigated ultrafast phonon dynamics, and it was found that the major part of the lost angular momentum from the spin system is transferred to the lattice on subpicosecond time scales. However, attempts of calculation to estimate the demagnetization rate on the basis of electron-phonon scattering [15–19] were unsuccessful in reproducing the large demagnetization observed experimentally.

Carpene *et al.* [9] argued that the demagnetization is determined by magnon emission, where the electron-magnon scattering can transfer angular momentum from the spin to

the orbital magnetic moment, which is immediately quenched by the crystal field. However, it was found that the calculated demagnetization rate for Fe and Ni, when considering only magnon emission, is too small compared to the experimental values [18]. Haag *et al.* [20] suggested that neither electron scattering from phonons nor electron scattering from magnons can independently explain experimental demagnetization rates, while a combination of both processes could. Some reports also provide indirect evidence of ultrafast magnon emission [21–27], while the role of magnons for the efficiency of ultrafast demagnetization was not addressed.

With the development of tabletop extreme ultraviolet (XUV) sources with pulse durations of <30 fs, in-house investigations of element-selective magnetization dynamics have become possible [28–30]. The elemental specificity can be used for separating the dynamical response of constituents in alloys or in layered magnetic structures. Further, the ability of simultaneously accessing the response of different constituents provides additional information on the involved mechanism in the microscopic processes, such as interatomic and interlayer exchange interaction. In Ref. [28], element-resolved measurements of demagnetization dynamics in permalloy (Py) revealed a delay in the onset of Ni demagnetization relative to that of Fe. This finding has later been confirmed by us and others [29,30]. Recently, the delay was also found between Fe and Ni at the L edges in the soft x-ray regime [31]. Furthermore, when Py was alloyed with 40% Cu, it was found that the observed delay increased by a factor inversely proportional to the exchange interaction. On the basis of these results, the authors of Ref. [28] hypothesize the role of the exchange interaction in the observed delay by assuming that the Fe sublattice participates in the direct

---

*Present address: Max-Born-Institut für Nichtlineare Optik und Kurzzeitspektroskopie, Max-Born-Straße 2A, 12489 Berlin, Germany; sj.phys@gmail.com

†Corresponding author: ronny.knut@physics.uu.se

demagnetization process while Ni demagnetizes through the exchange interaction with Fe.

In this Letter, we present measurements of the element-specific demagnetization in a series of $Fe_{1-x}Ni_x$ alloys with six different compositions. A composition-dependent variation in the relative delay between the onset of the Fe and Ni demagnetization is observed. The relative delay is found to follow the trend of the inverse of Curie temperature. The experimental demagnetization is fitted using a model describing preferential magnon scattering in the Fe sublattice which provides values for the spin wave stiffness (D_{spin}) in each alloy composition [32]. The D_{spin} values extracted from the fits correspond well to calculated *ab initio* values, values derived from the Bloch $T^{3/2}$ law, and values of the exchange stiffness obtained from neutron scattering [33].

Samples with the geometry Si(substrate)/Ta(2 nm)/Fe_{1-x} Ni_x(20 nm)/Ta(2 nm) and with nominal concentrations of $x =$ 0.0, 0.2, 0.3, 0.4, 0.6, 0.7, 0.8, 1.0 were produced by magnetron sputtering. Rutherford backscattering spectrometry was performed to determine the actual compositions and thicknesses of the alloy layer. The concentrations were determined to be 20%, 30%, 36%, 58%, 68%, and 78% Ni. The thickness of the FeNi alloy layer was determined to 17.5 ± 0.9 nm. All the samples were characterized by x-ray diffraction (XRD) [see the Supplemental Material (SM) [34] and Refs. [35,36] therein). XRD confirms a single phase for all samples, with body-centered-cubic (bcc) structures for $x =$ 0.0, 0.2, 0.3, 0.36 and face-centered-cubic (fcc) structures for $x = 0.58, 0.68, 0.78, 1.0$.

The theoretical spin wave stiffness [37] is obtained in terms of total exchange constant J_{0j}, obtained from first-principles calculations (see SM [34] and Refs. [38,39] therein)

$$D_{spin} = \lim_{\eta \to 0} D(\eta)$$
$$= \frac{2\mu_B}{3M} \sum_{0 < R_{0j} < R_{max}} J_{0j} R_{0j}^2 \exp(-\eta R_{0j}/a) \qquad (1)$$

implemented in the Uppsala atomistic spin dynamics code (UppASD) [40]. In Eq. (1), $R_{0j} = |\mathbf{R}_{0j}|$ denotes the distance between atomic sites. R_{max} denotes the radius cutoff that was chosen large enough to converge, M is the average magnetic moment, a is the lattice parameter, and η is a parameter to ensure the convergence of the sum.

Our experimental setup for studying ultrafast demagnetization consists of a femtosecond near-infrared (NIR) laser (800 nm, 35 fs, 0.8 mJ, 10 KHz), where 80% of the light is focused into a He-filled gas cell for high harmonic generation (HHG). This produces ultrashort XUV pulses that retain the polarization and coherence of the driving NIR [41]. The generated p-polarized XUV pulses, with energies ranging from 40 to 72 eV, are focused on the sample at an incidence angle of $45°$. A grating spectrometer spectrally resolves the reflected XUV on a position sensitive multichannel plate detector [see resulting spectra in Fig. 1(a)]. The high-energy cutoff is due to an Al filter after the gas cell that reflects the NIR and only transmits XUV energies below 72 eV. The magnetization is probed in the transverse magneto-optical Kerr effect (T-MOKE) geometry by calculating the asymmetry parameter [$A(E)$], defined as the normalized difference spectrum of the reflected intensities [$I_p^{\pm}(E)$] measured for opposite magnetic
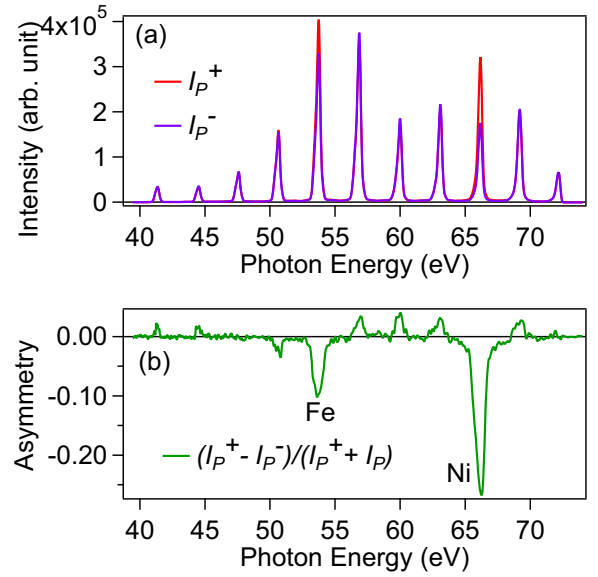

FIG. 1. (a) Reflected XUV spectra collected for two opposite in-plane magnetization directions for a nondemagnetized state of $Fe_{0.22}Ni_{0.78}$. (b) Asymmetry spectrum obtained from (a).

field directions, applied parallel to the sample surface and perpendicular to the plane of the incidence,

$$A(E) = \frac{I_p^+(E) - I_p^-(E)}{I_p^+(E) + I_p^-(E)}, \qquad (2)$$

where E is the photon energy of the XUV. A fraction of the remaining 800 nm light of the laser is used as a pump-pulse for demagnetizing the sample. Since the pump and probe pulses originate from the same initial laser pulse, the temporal jitter is practically eliminated. An optical delay stage is used to introduce a controllable delay between the NIR pump and the XUV probe. The experimental setup is described in detail in Refs. [42], [30], and [43].

Typical reflectivity spectra are shown in Fig. 1(a), obtained with two opposite magnetization directions for Py ($Fe_{0.22}Ni_{0.78}$). The odd harmonics are well separated from each other by 3.1 eV, so the asymmetry can be measured as a function of harmonic energy without ambiguity. The corresponding asymmetry spectrum is shown in Fig. 1(b). The asymmetry is strongly enhanced near 54 and 66 eV, corresponding to the Fe and Ni $M_{2,3}$ absorption edges, respectively. Since to a first-order approximation the asymmetry is proportional to the magnetization [44], the elemental magnetization can be obtained from the asymmetry at the absorption edges. The simultaneous recording of the whole spectrum enables detecting relative dynamics between the elements without experimental artifacts from jitter and drift. Pump-probe measurements were performed for all samples. In Figs. 2(a) and 2(b), the normalized asymmetry at the Fe and Ni $M_{2,3}$ edges are plotted as a function of delay between the pump and probe for two compositions (other compositions are presented in the SM). All compositions display a delay in the onset of Ni demagnetization relative to Fe. The pump fluence was maintained such that the maximum demagnetization is about 30%–40% for all samples. The delayed response of Ni rel-
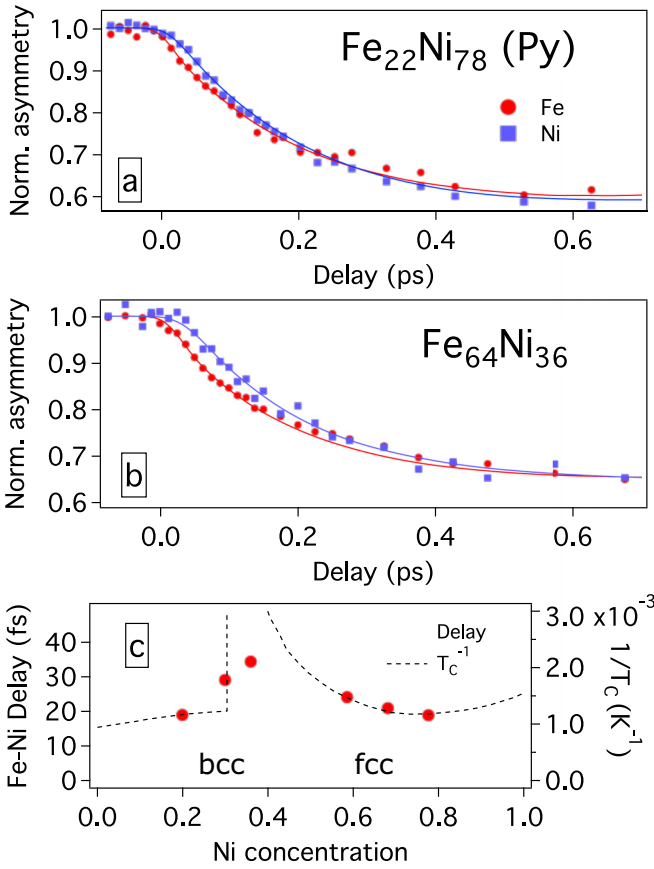
FIG. 2. Asymmetry obtained at Fe $M_{2,3}$ ($\sim$54 eV) and Ni $M_{2,3}$ ($\sim$66 eV) edges are plotted (red circles for Fe and blue squares for Ni) with the pump-probe delay in (a) and (b) for compositions x = 0.78 and 0.36, respectively. The lines through the experimental data points are the fitted curves using the magnon diffusion model. (c) The inverse transition temperature [45] and the extracted delay in Ni demagnetization relative to that of Fe are plotted versus the compositional variation.

ative to Fe (Fe-Ni delay) is quantified by shifting the Fe demagnetization and calculating the root mean square (RMS) of the difference between Fe and Ni demagnetizations. The shift that provides the lowest RMS, within a 150-fs window around the onset of the demagnetization is given as the Fe-Ni delay. The results are shown in Fig. 2(c) for the different compositions. For a Ni concentration of 78% the delay is 19 fs, which is close to what has been reported in earlier studies [28,30] for Py. Starting from a high Ni concentration, the delay first shows an increase, peaks around 40% Ni, and then decreases for lower Ni concentrations. The inverse of the calculated Curie temperature [45] is plotted along the compositions on the right axis of Fig. 2(c), indicating a correlation between the average exchange interaction of the samples and the Fe-Ni delay. In order to eliminate any delay resulting from artifacts, we have simultaneously measured the demagnetization of elemental Fe and Ni in a reference sample. The reference sample consisting of elemental Fe and Ni grown on the same substrate exhibits no delayed demagnetization response, unambiguously proving that the observed effect is a consequence of alloy-

ing (see SM [34]). This result agrees qualitatively with the strength of the exchange interaction in Fe$_{1-x}$Ni$_x$ alloys as discussed in Ref. [28]. However, a quantitative correlation between the delay and any material parameter is absent as the microscopic mechanism that is involved in the angular momentum transfer during the ultrafast demagnetization is lacking.

The delayed response in the Ni sublattice in Cu-permalloy system is explained by ultrafast magnon generation that occurs predominantly in the Fe sublattice by Knut *et al.* [32]. The spatially inhomogeneous magnon distribution, at short timescales, would diffuse and increase the magnon population in the Ni sublattice at longer timescales. This would be manifested as a delayed demagnetization in the Ni sublattice. Note that the demagnetization is still driven by other processes, such as EY-spin flips, since the magnon generation is considered to be primarily spin conserving. In Figs. 2(a) and 2(b) the solid lines represent fits using this magnon diffusion model [32]. In this model, the inhomogeneous magnon distribution is generated by a nonuniform exchange scattering, mediated by the sd-exchange interaction ($J^{sd}_{\text{Fe,Ni}}$). The spatial distribution of the magnon amplitude is determined by the Hamiltonian, $H = H_0 + H_1$, where $H_0 = -2\sum_{i<j} J_{ij}S_i \cdot S_j$, is the exchange interaction between the atomic sites i and j, and $H_1 = -2\sum_j J^{sd}_j s_i \cdot S_j$ accounts for the element-dependent exchange interaction between the free (s) and localized (S_j) spins. The solution of the Hamiltonian results in a magnon probability distribution that is proportional to the square of the sd-exchange interaction ($J^{sd}_{\text{Fe,Ni}}$) and hence it is spatially inhomogeneous at time zero according to the Fe, Ni distribution. The time evolution is then obtained by introducing the magnon dispersion relation $\omega(k) = 2D_{\text{spin}}(1 - \cos(k.L))/\hbar L^2$ (D_{spin} is the spin wave stiffness, k is the wave vector, and L is the lattice parameter) in the phase of the Fourier components of the spatially inhomogeneous amplitude. The time evolution should mainly be determined by the time it takes for a magnon to diffuse from one atom to its nearest neighbors, which is determined by the shortest distance between the atoms and the spin wave stiffness. Since the nearest-neighbor distance for bcc Fe (0.2482 nm) and fcc Ni (0.2495 nm) is almost the same, the bcc-to-fcc transition should have no effect in this model. Here, we assume that the ratio of exchange scattering is independent of the Ni concentration and use the value of $J^{sd}_{\text{Fe}}/J^{sd}_{\text{Ni}} = 2.2$ for all samples. Note that a ratio of 1 would result in a homogenous magnon distribution, with no delayed demagnetization of Ni. All other parameters are the same as used for Py in Ref. [32]. Since $J^{sd}_{\text{Fe}}/J^{sd}_{\text{Ni}}$ is kept fixed, the only free parameter that directly affects the delayed demagnetization of Ni is the spin wave stiffness (D_{spin}). In Fig. 3, the fitted value of the spin wave stiffness (solid blue squares) is plotted versus the Ni concentration together with reference data obtained from neutron scattering experiments (solid red circles) [33]. Furthermore, the spin-wave stiffness was also extracted from the temperature-dependent saturation magnetization $m_s(T)$ (black circles) by fitting to the Bloch $T^{3/2}$ law; $[m_s(0) - m_s(T)] \propto (k_B T/D_{\text{spin}})^{3/2}$ in the temperature range of 10–150 K, where T is temperature and k_B is Boltzmann constant. For details see the SM [34] and Ref. [46]. Finally, we also show *ab initio* calculated values of the spin-wave stiffness (green squares). The derived values of D_{spin} from the simula-
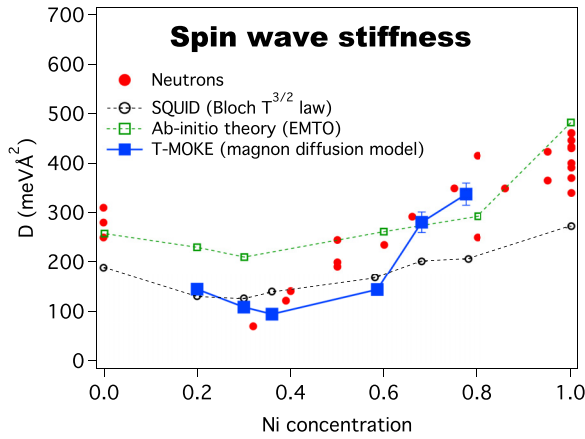
FIG. 3. Spin wave stiffness obtained from the element specific demagnetization curves, saturation magnetization, theoretical calculation, and neutron scattering results [33] are plotted with the Ni concentrations in $Fe_{1-x}Ni_x$ alloy.

tion of inhomogeneous magnon scattering are similar to the values obtained by other methods. Strikingly, the general trend of D_{spin} is similar for all the different methods of extracting the spin-wave stiffness. It is clear that the spin-wave stiffness decreases when pure Ni is alloyed with Fe. The minimum value is observed around the bcc-to-fcc phase transition (35% Ni) [47], after which it increases for higher Fe concentrations. Note that the fixed value of $J_{Fe}^{sd}/J_{Ni}^{sd} = 2.2$ was chosen to provide a reasonable correspondence to neutron scattering data for Py, however, there was no adjustable parameter for the other alloy concentrations. The calculated magnon scattering

rate in Fe by Haag *et al.* [20] is an order of magnitude higher than in Ni, suggesting that the ratio of 2.2 in Fe-Ni alloys is a reasonable value.

In conclusion, element-specific demagnetization dynamics in $Fe_{1-x}Ni_x$ alloys were measured using the time-resolved T-MOKE technique with ultrashort XUV pulses. A delay in the onset of the Ni demagnetization, relative to that of Fe, was observed for all studied compositions. This delay is inherent to Fe-Ni alloys, and is not observed for elemental Fe and Ni. The delay was found to be correlated with the inverse of the Curie temperature across the whole compositions range. We find that the Fe and Ni demagnetizations are well described by an ultrafast inhomogeneous magnon scattering. By adopting a higher magnon generation rate at Fe sites compared to Ni sites, we extract the spin-wave stiffness for all compositions which are in excellent agreement with the values obtained from neutron scattering measurement, static magnetization data, and *ab initio* calculations.

[1] E. Beaurepaire, J.-C. Merle, A. Daunois, and J.-Y. Bigot, Ultrafast Spin Dynamics in Ferromagnetic Nickel, Phys. Rev. Lett. **76**, 4250 (1996).

[2] F. Dalla Longa, J. T. Kohlhepp, W. J. M. de Jonge, and B. Koopmans, Influence of photon angular momentum on ultrafast demagnetization in nickel, Phys. Rev. B **75**, 224431 (2007).

[3] J.-Y. Bigot, M. Vomir, and E. Beaurepaire, Coherent ultrafast magnetism induced by femtosecond laser pulses, Nat. Phys. **5**, 515 (2009).

[4] A. J. Schellekens, W. Verhoeven, T. N. Vader, and B. Koopmans, Investigating the contribution of superdiffusive transport to ultrafast demagnetization of ferromagnetic thin films, Appl. Phys. Lett. **102**, 252408 (2013).

[5] M. Battiato, K. Carva, and P. M. Oppeneer, Theory of laser-induced ultrafast superdiffusive spin transport in layered heterostructures, Phys. Rev. B **86**, 024404 (2012).

[6] G. P. Zhang and W. Hübner, Laser-Induced Ultrafast Demagnetization in Ferromagnetic Metals, Phys. Rev. Lett. **85**, 3025 (2000).

[7] B. Y. Mueller, T. Roth, M. Cinchetti, M. Aeschlimann, and B. Rethfeld, Driving force of ultrafast magnetization dynamics, New J. Phys. **13**, 123010 (2011).

[8] T. Roth, A. J. Schellekens, S. Alebrand, O. Schmitt, D. Steil, B. Koopmans, M. Cinchetti, and M. Aeschlimann, Temperature

Dependence of Laser-Induced Demagnetization in Ni: A Key for Identifying the Underlying Mechanism, Phys. Rev. X **2**, 021006 (2012).

[9] E. Carpene, E. Mancini, C. Dallera, M. Brenna, E. Puppin, and S. De Silvestri, Dynamics of electron-magnon interaction and ultrafast demagnetization in thin iron films, Phys. Rev. B **78**, 174422 (2008).

[10] M. Krauß, T. Roth, S. Alebrand, D. Steil, M. Cinchetti, M. Aeschlimann, and H. C. Schneider, Ultrafast demagnetization of ferromagnetic transition metals: The role of the coulomb interaction, Phys. Rev. B **80**, 180407(R) (2009).

[11] B. Koopmans, G. Malinowski, F. Dalla Longa, D. Steiauf, M. Fahnle, T. Roth, M. Cinchetti, and M. Aeschlimann, Explaining the paradoxical diversity of ultrafast laser-induced demagnetization, Nat. Mater. **9**, 259 (2010).

[12] C. Dornes, Y. Acremann, M. Savoini, M. Kubli, M. J. Neugebauer, E. Abreu, L. Huber, G. Lantz, C. A. F. Vaz, H. Lemke, E. M. Bothschafter, M. Porer, V. Esposito, L. Rettig, M. Buzzi, A. Alberca, Y. W. Windsor, P. Beaud, U. Staub, D. Zhu *et al.*, The ultrafast Einstein–de Haas effect, Nature (London) **565**, 209 (2019).

[13] P. Maldonado, T. Chase, A. H. Reid, X. Shen, R. K. Li, K. Carva, T. Payer, M. Horn von Hoegen, K. Sokolowski-Tinten, X. J. Wang, P. M. Oppeneer, and H. A. Dürr, Tracking the ultrafast nonequilibrium energy flow between electronic and

lattice degrees of freedom in crystalline nickel, Phys. Rev. B **101**, 100302(R) (2020).

[14] S. R. Tauchert, M. Volkov, D. Ehberger, D. Kazenwadel, M. Evers, H. Lange, A. Donges, A. Book, W. Kreuzpaintner, U. Nowak, and P. Baum, Polarized phonons carry angular momentum in ultrafast demagnetization, Nature (London) **602**, 73 (2022).

[15] S. Essert and H. C. Schneider, Electron-phonon scattering dynamics in ferromagnetic metals and their influence on ultrafast demagnetization processes, Phys. Rev. B **84**, 224405 (2011).

[16] K. Carva, M. Battiato, and P. M. Oppeneer, *Ab Initio* Investigation of the Elliott-Yafet Electron-Phonon Mechanism in Laser-Induced Ultrafast Demagnetization, Phys. Rev. Lett. **107**, 207201 (2011).

[17] K. Carva, M. Battiato, D. Legut, and P. M. Oppeneer, Ab initio theory of electron-phonon mediated ultrafast spin relaxation of laser-excited hot electrons in transition-metal ferromagnets, Phys. Rev. B **87**, 184425 (2013).

[18] C. Illg, M. Haag, and M. Fähnle, Ultrafast demagnetization after laser irradiation in transition metals: Ab initio calculations of the spin-flip electron-phonon scattering with reduced exchange splitting, Phys. Rev. B **88**, 214404 (2013).

[19] B. Y. Mueller, A. Baral, S. Vollmar, M. Cinchetti, M. Aeschlimann, H. C. Schneider, and B. Rethfeld, Feedback Effect during Ultrafast Demagnetization Dynamics in Ferromagnets, Phys. Rev. Lett. **111**, 167204 (2013).

[20] M. Haag, C. Illg, and M. Fähnle, Role of electron-magnon scatterings in ultrafast demagnetization, Phys. Rev. B **90**, 014417 (2014).

[21] A. B. Schmidt, M. Pickel, M. Donath, P. Buczek, A. Ernst, V. P. Zhukov, P. M. Echenique, L. M. Sandratskii, E. V. Chulkov, and M. Weinelt, Ultrafast Magnon Generation in an Fe Film on Cu(100), Phys. Rev. Lett. **105**, 197401 (2010).

[22] R. Gort, K. Bühlmann, S. Däster, G. Salvatella, N. Hartmann, Y. Zemp, S. Holenstein, C. Stieger, A. Fognini, T. U. Michlmayr, T. Bähler, A. Vaterlaus, and Y. Acremann, Early Stages of Ultrafast Spin Dynamics in a 3*d* Ferromagnet, Phys. Rev. Lett. **121**, 087206 (2018).

[23] E. Carpene, H. Hedayat, F. Boschini, and C. Dallera, Ultrafast demagnetization of metals: Collapsed exchange versus collective excitations, Phys. Rev. B **91**, 174414 (2015).

[24] U. Atxitia, O. Chubykalo-Fesenko, J. Walowski, A. Mann, and M. Münzenberg, Evidence for thermal mechanisms in laser-induced femtosecond spin dynamics, Phys. Rev. B **81**, 174401 (2010).

[25] M. Cinchetti, M. Sánchez Albaneda, D. Hoffmann, T. Roth, J.-P. Wustenberg, M. Krauß, O. Andreyev, H. C. Schneider, M. Bauer, and M. Aeschlimann, Spin-Flip Processes and Ultrafast Magnetization Dynamics in Co: Unifying the Microscopic and Macroscopic View of Femtosecond Magnetism, Phys. Rev. Lett. **97**, 177201 (2006).

[26] E. Turgut, D. Zusin, D. Legut, K. Carva, R. Knut, J. M. Shaw, C. Chen, Z. Tao, H. T. Nembach, T. J. Silva, S. Mathias, M. Aeschlimann, P. M. Oppeneer, H. C. Kapteyn, M. M. Murnane, and P. Grychtol, Stoner versus Heisenberg: Ultrafast exchange reduction and magnon generation during laser-induced demagnetization, Phys. Rev. B **94**, 220408(R) (2016).

[27] S. Eich, M. Plötzing, M. Rollinger, S. Emmerich, R. Adam, C. Chen, H. C. Kapteyn, M. M. Murnane, L. Plucinski, D. Steil, B. Stadtmüller, M. Cinchetti, M. Aeschlimann, C. M. Schneider, and S. Mathias, Band structure evolution during the ultrafast ferromagnetic-paramagnetic phase transition in cobalt, Sci. Adv. **3**, e1602094 (2017).

[28] S. Mathias, C. La-O-Vorakiat, P. Grychtol, P. Granitzka, E. Turgut, J. M. Shaw, R. Adam, H. T. Nembach, M. E. Siemens, S. Eich, C. M. Schneider, T. J. Silva, M. Aeschlimann, M. M. Murnane, and H. C. Kapteyn, Probing the timescale of the exchange interaction in a ferromagnetic alloy, Proc. Natl. Acad. Sci. USA **109**, 4792 (2012).

[29] S. Günther, C. Spezzani, R. Ciprian, C. Grazioli, B. Ressel, M. Coreno, L. Poletto, P. Miotti, M. Sacchi, G. Panaccione, V. Uhlir, E. E. Fullerton, G. De Ninno, and C. H. Back, Testing spin-flip scattering as a possible mechanism of ultrafast demagnetization in ordered magnetic alloys, Phys. Rev. B **90**, 180407(R) (2014).

[30] S. Jana, J. A. Terschlüsen, R. Stefanuik, S. Plogmaker, S. Troisi, R. S. Malik, M. Svanqvist, R. Knut, J. Söderström, and O. Karis, A setup for element specific magnetization dynamics using the transverse magneto-optic Kerr effect in the energy range of 30-72 eV, Rev. Sci. Instrum. **88**, 033113 (2017).

[31] S. Jana, R. Knut, S. Muralidhar, R. S. Malik, R. Stefanuik, J. Åkerman, O. Karis, C. Schüßler-Langeheine, and N. Pontius, Experimental confirmation of the delayed Ni demagnetization in FeNi alloy, Appl. Phys. Lett. **120**, 102404 (2022).

[32] R. Knut, E. K. Delczeg-Czirjak, S. Jana, J. M. Shaw, H. T. Nembach, Y. Kvashnin, R. Stefanuik, R. S. Malik, P. Grychtol, D. Zusin *et al.*, Inhomogenious magnon scattering during ultrafast demagnetization, arXiv:1810.10994.

[33] C. A. F. Vaz, J. A. C. Bland, and G. Lauhoff, Magnetism in ultrathin film structures, Rep. Prog. Phys. **71**, 056501 (2008).

[34] Supplemental Material can be found at http://link.aps.org/supplemental/10.1103/PhysRevB.107.L180301, which contains details about the sample preparation and characterization, extracting spin-wave stiffness from Bloch's 3/2 law and first-principle calculation, additional data and obtained parameters from fitting.

[35] B. Glaubitz, S. Buschhorn, F. Brüssing, R. Abrudan, and H. Zabel, Development of magnetic moments in $Fe_{1-x}Ni_x$ alloys, J. Phys.: Condens. Matter **23**, 254210 (2011).

[36] Y. Guang-Hua, R. Ting-Ting, L. Ming-Hua, Z. Feng-Wu, J. Huang-Wei, and L. Wu-Yan, Dead layer in a Ta/Ni81Fe19/Ta structure, Chin. Phys. Lett. **19**, 1347 (2002).

[37] M. Pajda, J. Kudrnovský, I. Turek, V. Drchal, and P. Bruno, Ab initio calculations of exchange interactions, spin-wave stiffness constants, and curie temperatures of Fe, Co, and Ni, Phys. Rev. B **64**, 174402 (2001).

[38] A. I. Liechtenstein, M. I. Katsnelson, and V. A. Gubanov, Exchange interactions and spin-wave stiffness in ferromagnetic metals, J. Phys. F **14**, L125 (1984).

[39] P. Soven, Coherent-potential model of substitutional disordered alloys, Phys. Rev. **156**, 809 (1967).

[40] B. Skubic, J. Hellsvik, L. Nordström, and O. Eriksson, A method for atomistic spin dynamics simulations: Implementation and examples, J. Phys.: Condens. Matter **20**, 315203 (2008).

[41] P. B. Corkum, Plasma Perspective on Strong Field Multiphoton Ionization, Phys. Rev. Lett. **71**, 1994 (1993).

[42] S. Plogmaker, J. A. Terschlüsen, N. Krebs, M. Svanqvist, J. Forsberg, U. B. Cappel, J.-E. Rubensson, H. Siegbahn, and J. Söderström, Helios—A laboratory based on high-order harmonic generation of extreme ultraviolet photons for time-resolved spectroscopy, Rev. Sci. Instrum. **86**, 123107 (2015).

[43] R. Stefanuik, R. Knut, S. Jana, J. A. Terschlüsen, A. Sandell, and J. Söderström, Developments and enhancements to the helios pump probe system, J. Electron Spectrosc. Relat. Phenom. **224**, 33 (2018).

[44] C. La-O-Vorakiat, E. Turgut, C. A. Teale, H. C. Kapteyn, M. M. Murnane, S. Mathias, M. Aeschlimann, C. M. Schneider, J. M. Shaw, H. T. Nembach, and T. J. Silva, Ultrafast Demagnetization Measurements Using Extreme Ultraviolet Light: Comparison of Electronic and Magnetic Contributions, Phys. Rev. X **2**, 011005 (2012).

[45] Y. Kakehashi, Systematic variations of magnetic properties in 3d transition metal alloys, Prog. Theor. Phys. Suppl. **101**, 105 (1990).

[46] H. T. Nembach, J. M. Shaw, M. Weiler, E. Jue, and T. J. Silva, Linear relation between Heisenberg exchange and interfacial Dzyaloshinskii-Moriya interaction in metal films, Nat. Phys. **11**, 825 (2015).

[47] M. A. W. Schoen, J. Lucassen, H. T. Nembach, B. Koopmans, T. J. Silva, C. H. Back, and J. M. Shaw, Magnetic properties in ultrathin 3d transition-metal binary alloys. II. Experimental verification of quantitative theories of damping and spin pumping, Phys. Rev. B **95**, 134411 (2017).